Catalyst Design to Address Nylon Plastics Recycling

Liwei Ye,[a] Xiaoyang Liu,[b] Kristen Beckett,[a] Jacob O. Rothbaum,[a] Clarissa Lincoln,[c][d] Linda J. Broadbelt,*[b] Yosi Kratish,*[a] and Tobin J. Marks*[a]

[a] Department of Chemistry, Northwestern University, 2145 Sheridan Road, Evanston, IL 60208-3113, United States.
[b] Department of Chemical and Biological Engineering, Northwestern University, 2145 Sheridan Road, Evanston, IL 60208-3113, United States.
[c] Renewable Resources and Enabling Sciences Center, National Renewable Energy Laboratory, Golden, CO 80401, United States.
[d] BOTTLE Consortium, National Renewable Energy Laboratory, Golden, CO 80401, United States.

ABSTRACT: Rational tailoring of catalytic systems offers highly desirable transformations targeting the growing environmental challenges associated with plastics pollution. For example, the identification of efficient catalysts to address alarming end-of-life Nylon pollution remains underexplored. Nylon-6 is a non-biodegradable high-performance engineering plastic with centuries of chemical persistence, resulting in millions of tons of waste accumulation. Here we report the rational manipulation of organolanthanide catalyst structure to achieve an exceptionally efficient, solventless, and scalable Nylon-6 depolymerization process, affording monomer ε-caprolactam in ≥99% yield. Specifically, catalyst $Cp^*_2LaCH(TMS)_2$ ($Cp^* = \eta^5\text{-}C_5Me_5$, $TMS = SiMe_3$) operates at catalyst loadings as low as 0.2 mol% and temperatures as low as 220 °C. For efficient deconstruction of more recalcitrant commodity Nylon-6 end-of-life articles such as fishing nets, carpets, and clothing, the robust, thermally stable *ansa*-metallocene catalyst $Me_2SiCp''_2YCH(TMS)_2$, ($Cp'' = \eta^5\text{-}C_5Me_4$) effects >99% conversion of these items into ε-caprolactam. The collected product can be readily re-polymerized to afford pristine Nylon-6 with higher molecular masses and comparable structural regularity, providing a superior upcycling pathway for end-of-life Nylon plastics. Experimental mechanistic studies reveal intriguing and effective depolymerization pathways, such as catalytic intrachain "unzipping" enabled by the catalyst π-ancillary ligand steric constraints. Effective interchain "hopping" mechanisms, as well as chain-end deactivation are also demonstrated and supported by DFT analyses.

INTRODUCTION

Catalysis is central to countless chemical transformations and holds great promise for the efficient recycling of commodity plastics.[1–3] Plastics are ubiquitous, versatile, and low-cost polymeric materials that have dramatically enhanced the quality of human life for more than a century. Currently, plastics are being produced at an annual rate of 450 million tons, which is projected to double by 2045.[4] Nevertheless, with only limited tools available to address plastics end-of-life, their accumulation has emerged as a global environmental challenge.[5,6] For example, Nylons (or polyamides), which are produced on a scale exceeding 8.9 million tons annually,[7] significantly contribute to the non-degradable plastic waste pollution in oceans and landfills, reflecting their superior chemical robustness and lack of effective recycling technologies.[8] Indeed, it is estimated that by 2050, plastic waste will outweigh fish in the ocean,[9] with Nylon-6 contributing ca. 10% of ocean plastic pollution as discarded/lost fishing nets (so-called "ghost nets").[10] This amounts to >600,000 tons of abandoned fishing nets annually.[11,12] Nylons are the most prevalent polymers in the stomachs of marine animals, illustrating the Nylon persistence challenge to the global marine ecosystems.[13]

Since discovery by Schlack in 1938,[14] Nylon-6 has emerged as a versatile thermoplastic with widespread application in the automotive, packaging, carpet, and textile industries,[15] as well as in fishing gear. Industrially, Nylon-6 is readily prepared from ε-caprolactam via water-assisted ring-opening polymerization or anionic ring-opening polymerization (ROP) using acylated caprolactam as initiator.[14] Nylon-6 commercial products dominate the global Nylon market with more than 50% of the total revenue,[7] and a market size projected to exceed $21 billion by 2026.[16,17]

Despite the attractions of Nylon-6, including high tensile strength, rigidity, toughness, as well as thermal and abrasion resistance,[14,15,18] end-of-life management of Nylon waste falls far below the worldwide production rate.[8,19,20] Specifically, traditional methods to partially recover the energy stored in plastics waste such as incineration and pyrolysis, in the case of Nylons release toxic/harmful gases including CO, NH_3, and CO_2, further exacerbating the environmental challenges.[21] Furthermore, mechanical recycling of Nylons induces substantial properties deterioration, reflecting the elevated required temperatures, and is considered economically less attractive than for polyethylene terephthalate (PET).[11,22]

If efficient, chemical recycling of Nylon-6 could provide an attractive route back to ε-caprolactam, which is conventionally derived from fossil feedstocks, contributing to greenhouse gas emissions.[23,24] Conventionally, this process is performed under harsh conditions at elevated temperatures and high steam pressures, incurring high energy costs and has not been widely adopted industrially.[25] Very limited reports have described catalytic processes for Nylon-6 chemical recycling. For example, in a series of reports, Kamimura and Yamamoto et al studied the depolymerization of Nylon-6 in ionic liquids to produce ε-caprolactam in moderate yields (55-85%) with 5 wt% 4-dimethylaminopyridine (DMAP) as the catalyst.[26–28] However, this process requires > 300 °C reaction temperatures, since the crude product mixture contains large quantities of oligomers at lower reaction temperatures.[26] The decomposition of ionic liquids at high temperatures along with the high toxicity of DMAP pose additional limitations to this approach.[27,28] In 2020, Milstein et al reported a Ru-catalyzed depolymerization of Nylons to linear amino alcohols via hydrogenation (Figure 1A).[29] Nevertheless, even high 70 bar H_2 pressures and 48 h reaction times, this transformation does not produce ε-caprolactam. For Nylon-6, 24-48 % yields of 6-amino-1-hexanol are obtained.[27]

Recently, we reported in an initial screening study that tris[bis(trimethylsilyl)amido] lanthanide catalysts Ln^{NTMS} selectively depolymerize Nylon-6 powder to monomeric ε-caprolactam in a solvent-free process at 240-280 °C (Figure 1B).[30] Although >90 % yields of the ε-caprolactam are achieved, a substantial 5 mol% of the lanthanum catalyst (La^{NTMS}, **1**) is required. Furthermore, catalyst **1** is volatile under the reaction conditions and sublimes from the reaction mixture if the Nylon-6 powder and the catalyst are not well-mixed before and during the polymer melting stage at reaction onset.[31] Consequently, **1** is most effective as a depolymerization catalyst for virgin Nylon-6 powder so that maximum polymer-catalyst surface contact is maintained. Thus, for **1** to be effective, commercial Nylon yarn must be cryogenically milled to provide moderate ε-caprolactam yields (78%). Considering the high catalyst loading required for Ln^{NTMS} mediated depolymerizations, the loss due to catalyst volatility, and the impracticality of large-scale cryogenic grinding, we sought more effective catalysts.

Here we report optimal metallocene catalysts which are far more effective for Nylon-6 depolymerization and applicable to diverse Nylon-6 waste products. We present the first study showing how catalysis design and fine-tuning can achieve, 1) Fundamental mechanism-based design of efficient Nylon-6 depolymerization catalysts and 2) Addressing practical challenges in the recycling of end-of-life Nylon plastics. The Nylon-6 deconstruction processes disclosed here proceed in high yields-- up to >99% yield of the re-polymerizable caprolactam monomer, can operate under

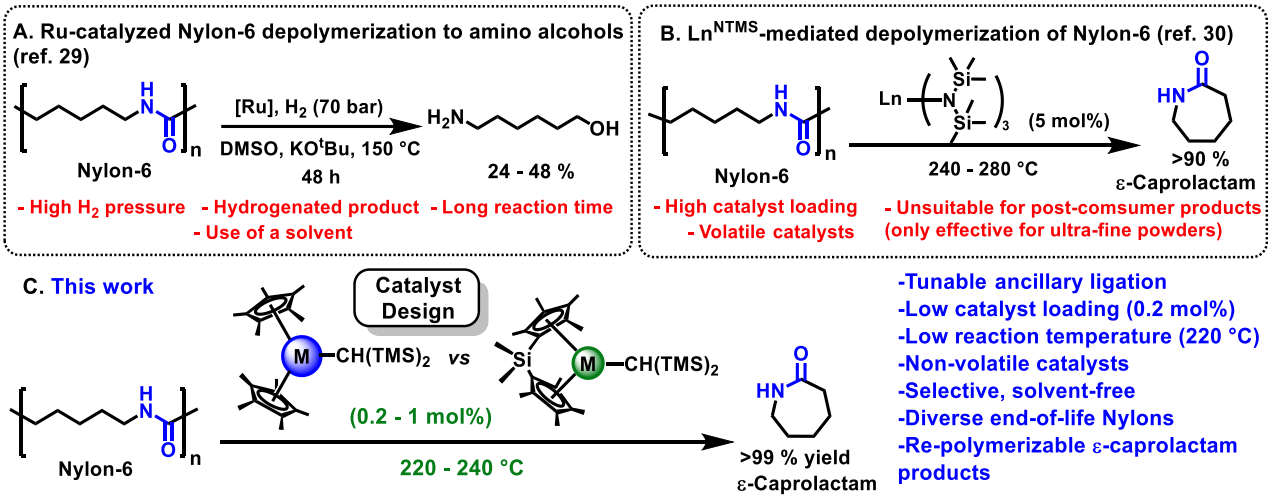

Figure 1. Recent examples of catalytic approaches to Nylon-6 chemical recycling.

mild conditions--lowest Nylon-6 to ε-caprolactam depolymerization temperature reported to date, 220 °C, while employing low catalyst loadings- as low as 0.2 mol%, and are compatible with a variety of post-consumer Nylon products (see below). Combined experimental and theoretical (DFT) mechanistic studies reveal rapid and highly selective catalytic processes, such as intrachain "unzipping" and interchain "hopping" mechanisms.

RESULTS AND DISCUSSION

Organolanthanide Catalyst Design

Commercial virgin Nylon-6 powder was first utilized to screen catalysts and catalytic conditions, to minimize/exclude the potential influence on depolymerization results reflecting poor polymer-catalyst contact, uneven mixing/heating, and plastic additives. The number average molecular weight (M_n) of the virgin Nylon-6 powder was determined to be 14,800 g mol^{-1} by Gel Permeation Chromatography (GPC). All depolymerizations were performed in a solventless mode, with crystalline ε-caprolactam collecting on the reactor cold wall (See Figure 2A and Figure S1).

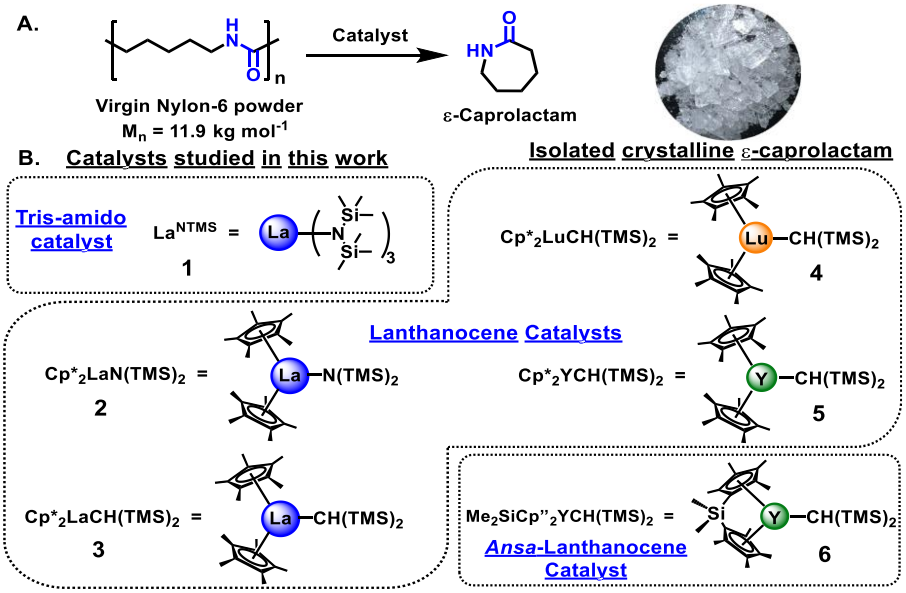

Figure 2. A. Reaction scheme for Nylon-6 depolymerization to ε-caprolactam. **B.** Structures of catalysts studied here.

In initial attempts to lower the catalyst loading of **1** from 5 mol% to 1 mol%, a moderate ε-caprolactam yield was obtained (69%, Table 1, entry 1) in 0.5 h reaction time at 240 °C. Further decreasing the catalyst loading of **1** to 0.2 mol% depressed the depolymerization yield to 5.6% (Table 1, entry 2), which prompted catalyst modification since efficient recycling will require lower catalyst loadings.[6,32] We hypothesized that, after depolymerization is initiated, the three reactive La-amide linkages might promote macromolecule crosslinking and catalyst immobilization (see more below for detailed mechanistic studies).

Thus, we envisioned tailoring the organolanthanide coordination sphere using non-dissociable ancillary π-ligands to sterically shield the highly electrophilic lanthanide centers while reducing impediments introduced by multiple reaction linkages. Note that lanthanocenes bearing a variety of non-dissociable supporting π-ligands such as bis(pentamethyl-cyclopentadienyl) (Cp^*_2) offer high coordinative

Table 1. Optimization of the catalytic Nylon-6 depolymerization conditions shown in **Figure 2A**.[a]

Entry	Catalyst	Catalyst loading (mol%)	Time (h)	Temperature (°C)	Yield (%)[b]
1	1	1.0	0.5	240	69
2	1	0.2	1.0	240	5.6
3	2	1.0	6.0	240	17
4	3	1.0	0.5	240	91
5	3	1.0	1.0	240	99
6	3	0.2	1.0	240	93
7	3	0.2	0.5	240	81
8[c]	3	0.2	3.0	240	97 (94)[d]
9	3	1.0	2.0	220	90
10	3	0.2	4.0	220	95
11	1	1.0	2.0	220	0
12	4	1.0	1.0	240	24
13	5	1.0	1.0	240	2.2
14	5	5.0	24	240	93
15	6	1.0	1.0	240	94
16	6	1.0	2.0	240	>99

[a] General depolymerization conditions: static vacuum (10^{-3} Torr), 100 mg of Nylon-6 powder in 50 mL Schlenk flask, unless otherwise stated. [b] Yields determined by ^{1}H NMR with a mesitylene internal standard. [c] Scaled-up depolymerization: 1.0 g of Nylon-6 in 100 mL Schlenk flask. [d] Isolated yield after recrystallization of product ε-caprolactam from hexane/acetone; see SI for details.

stability and a rich catalytic chemistry.[33] Here the La coordination sphere was first modified by replacing two -TMS_2N active sites with ancillary Cp* ligands ($Cp^*_2LaN(TMS)_2$, **2**). However, this led to a reduced depolymerization activity even with 1 mol% catalyst and an extended reaction time (17% in 6.0 h; Table 1, entry 3).

Next, $Cp^*_2LaCH(TMS)_2$ (**3**), which has previously been reported to efficiently catalyze C-N bond-forming reactions such as intramolecular cyclohydroaminations of aminoalkenes or aminoalkynes[34,35] was investigated for Nylon-6 depolymerization, which also involves an intramolecular cyclization to form C-N bonds. Strikingly, catalyst **3** is found to be a highly effective catalyst, at 1 mol% loading providing a 91% yield in only 0.5 h of reaction time at 240 °C (Table 1, entry 4). This result is a significant advance over catalyst **2**, demonstrating a key role for the sigma-bonded La ligand (from -$N(TMS)_2$ to - $CH(TMS)_2$) and is supported by DFT calculations (vide infra). Extending the reaction time from 0.5 h to 1 h affords an excellent yield of 99% for the **3**-mediated depolymerization (Table 1, entry 5). Additionally, **3** is found to be very active even with a lower catalyst loading of 0.2 mol% to provide a high yield of 93% (Table 1, entries 6,7), in marked contrast to catalyst **1** (5.6 % yield). To examine the scalability of this reaction, the **3**-mediated depolymerization was carried out on a gram scale using a 0.2 mol% catalyst loading. An NMR yield of 97% (94% isolated yield) was obtained (Table 1, entry 8).

Another consideration is the depolymerization reaction temperature. Chemical recycling of commodity polymers typically utilizes high reaction temperatures and therefore, is energy-intensive and may be accompanied by undesired thermal decomposition.[2,36] Although the present 240 °C reaction temperature is lower than typically reported for Nylon-6 depolymerization to ε-caprolactam (> 300 °C)[25,26,28,30], it is above the Nylon-6 (218.3 °C) melting point.[37] In an effort to lower the reaction temperature, catalytic studies were next conducted at 220 °C with 1 mol% catalyst **3** loading for 2 h with a respectable yield (Table 1, entry 9) and 95% yield for 4 h and 0.2 mol% catalyst loading (Table 1, entry 10). Note that this temperature is, to our knowledge, the lowest reported Nylon-6 depolymerization temperature under solvent-free conditions. In comparison, catalyst **1** is completely inactive at 220 °C (Table 1, entry 11).

Metal Ion Size and Ancillary Ligand Effects

To define any correlations between catalytic activity and Ln^{3+} radius,[38,39] the $Cp^*_2LnCH(TMS)_2$ homologs (Figure 2) where Ln = Lu (**4**; i.r. = 0.97 Å) and Y (**5**; i.r. = 1.01 Å) were prepared to compare with Ln = La (**3**; i.r. = 1.17 Å) Nylon-6 depolymerization characteristics. With 1 mol% loading, the Lu^{3+} catalyst affords lower ε-caprolactam yields (24%, Table 1, entry 12) in 1 h, while catalyst **5**, yields only 2.2% ε-caprolactam under identical reaction conditions (Table 1, entry 13), both substantially lower than that of catalyst **3** (99%; Table 1, entry 4). Achieving 93% yield of ε-caprolactam is possible with catalyst **5**, however, this requires a 5 mol% loading and 24 h (Table 1, entry 14). These results qualitatively and surprisingly parallel activity trends for Cp^*_2Ln-catalyzed olefin hydroelementation and other additions to C-C unsaturation.[34,35] They involve a mix of electronic and steric effects, with the later predominant and reflecting crowding in the insertive transition state.[35,40]

Nevertheless, smaller i.r. Y^{3+} metallocene complexes are known to display higher thermal stabilities, likely due to their low reactivities in undesired intramolecular thermolytic pathways.[34,41,42] Note also that Y lies at the lower end of the energy, cost,[43] and environmental impact scale,[44] and also displays significantly lower toxicity, reflected in a significantly higher median effect dose concentration (EC_{50}) of 6.7 μg/L *vs* that of La (EC_{50} = 147 μg/L).[45] In view of these factors we sought more effective Y catalysts by fine-tuning the Y coordination sphere.

Ansa-lanthanocenes such as $Me_2SiCp''_2Ln$- (Cp'' = η^5-Me_4C_5) with chelating ancillary π -ligands and larger "bite" angles (Figure 2) display substantially enhanced catalytic activities, such as in unsaturated carbon-carbon bond insertions into Ln-N bonds (10-100-fold increased TOFs).[46–48] Furthermore, the chelating *ansa*-bridged ligation should in principle further enhance the thermal robustness of Y catalytic systems.[49] Thus, $Me_2SiCp''_2YCH(TMS)_2$ (**6**) was prepared and examined for virgin Nylon-6 powder depolymerization.[48,50] Remarkably, "opening" of the Y coordination sphere dramatically increases the depolymerization yield

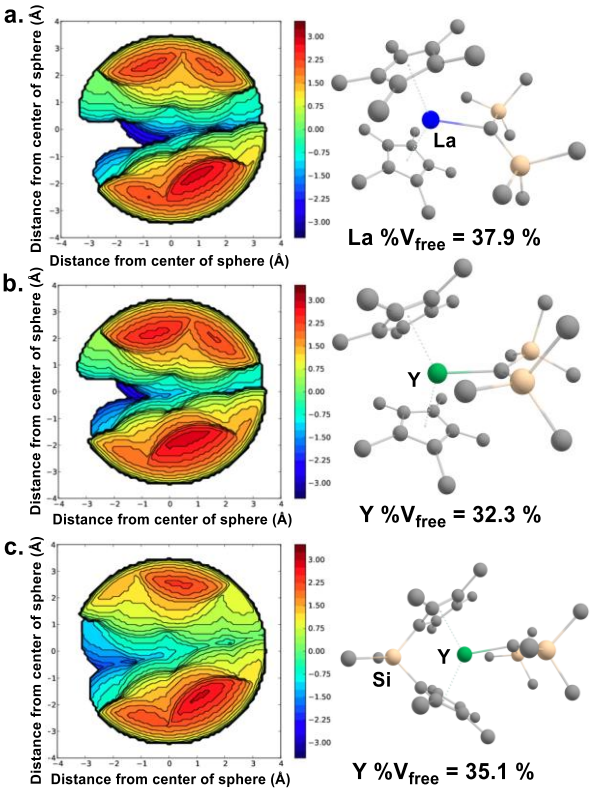

Figure 3. Computed percent free volume (%V_{free}) contours based on DFT-optimized structures for **a**. $Cp^*_2LaCH(TMS)_2$ (**3**); **b.** $Cp^*_2YCH(TMS)_2$ (**5**); and **c**. $Me_2SiCp''_2YCH(TMS)_2$ (**6**).

Table 2. Catalytic depolymerization of post-consumer Nylon plastics. [a]

Entry	Nylon plastic	Catalyst	Catalyst loading (mol%)	Time (h)	Yields (%)[b]
1	Fishing net	1	5.0	24	0
2	Fishing net	3	5.0	24	65
3	Fishing net	5	5.0	24	95
4	Fishing net	6	1.0	6.0	94
5	Carpet fiber	6	1.0	6.0	>99
6	Nylon yarn	6	1.0	6.0	87
7	T-shirt	6	1.0	6.0	99
8	Medical gloves [c]	6	1.0	12	89[d]
9	Fishing net + water bottle cap[e]	6	1.0	12	95

[a] General reaction conditions: static vacuum (10^{-3} Torr), 100 mg scissor-chopped end-of-life Nylon in 50 mL Schlenk flask. [b] Yields determined by ^{1}H NMR with mesitylene internal standard. [c] 355 mg sample of medical gloves, which contain 100 mg Nylon-6 (31%). [d] Determined from Nylon-6 content in medical glove sample; see SI for details. [e] Fishing net : water bottle cap in 1:1 mass ratio.

from 2% to 94% (Cp*$_2$Y- → Me$_2$SiCp''$_2$Y-) under identical reaction conditions (Table 1, entry 13 *vs* 15), illustrating the effects of ancillary ligand "engineering." Further extending the reaction time to 2 h effects a >99% conversion of Nylon-6 by catalyst **6** (Table 1, entry 16). This ligand manipulation essentially imbues a more desirable Y center with La center catalytic properties. This is also supported by steric effect quantification in free volume contours ($\%V_{free}$) computed for catalysts **3**, **5**, and **6** (Figure 3),[51] in strong parallel with their respective experimental activity trend.

Depolymerization of Post-Consumer Nylons

Encouraged by the high activities of lanthanocene catalysts **3** and **6** for finely powdered Nylon-6, the chemical recycling of "real-world" post-consumer Nylon-6 products was next examined (Table 2). These samples were manually chopped into smaller pieces, dried, and loaded into the aforementioned reaction flasks for depolymerization experiments (see SI for details). With relevance to ocean pollution, an end-of-life fishing net, used for 2 years, was first investigated. Beginning with catalyst **1**, it was found to rapidly sublime from the catalyst + finely chopped fishing net mixture, yielding negligible ε-caprolactam (Table 2, entry 1) after 24 h/ 240 °C. For catalyst **3**, the modest yield at high loadings observed (Table 2, entry 2) likely reflects poor mixing and the known thermal instability of this catalyst, while thermally more robust Y catalyst **5** delivers slightly higher yields (Table 2, entry 3), and coordinatively more open *ansa*-metallocene Y catalyst **6** achieves a remarkable 94% yield in only 6 h **(**Table 2, entry 4), paralleling the results with pristine powdered Nylon-6, arguably reflecting enhanced activity and thermal robustness.

To investigate the scope of **6**-catalyzed depolymerizations, other post-consumer Nylons were next examined. Carpet waste poses a global environmental impact.[52] With an annual carpet production of 12 billion feet^2 only 5% is recycled while 91% ends up in landfills; in the U.S. alone, 4 billion lb of carpet are discarded annually in landfills).[19,53] With an estimated that 75% of carpets composed of Nylon,[52,53] regenerating ε-caprolactam from carpet waste would be an ideal process. Pleasingly, a sample of carpet fiber was fully depolymerized with 1 mol% of **6**, providing a quantitative yield of ε-caprolactam (Table 2, entry 5). Next examined was post-consumer Nylon-6 yarn, which yielded 87% ε-caprolactam (Table 2, entry 6) under the same reaction conditions. Nylon fabrics, known for their durability and water resistance, are widely utilized in textiles to manufacture shirts, swimsuits, footwear, etc. A Nylon t-shirt was next cut into small pieces and subjected to depolymerization using catalyst **6**, producing ε-caprolactam with an impressive 99% yield (Table 2, entry 7).

To expand the scope of this sustainability study, we turned to pandemic-associated plastic pollution resulting from the enormous demand for medical plastics such as face masks and gloves to combat COVID-19.[54] A pair of Nylon medical gloves containing 31% of Nylon-6 was cut and subjected to polymer deconstruction with catalyst **6** (Table 2, entry 8). The **6**-mediated depolymerization of medical gloves furnished 89% yield of ε-caprolactam with respect to the Nylon content (see SI for details). Finally, in real-world marine plastic wastes, fishing net debris is typically mixed with other plastics such as containers, bags, straws, bottle caps, etc.[12] Besides Nylon wastes, polyolefins such as polyethylene and polypropylene (PE, PP) are the most common polymers in ocean plastics.[12] To investigate the applicability of catalyst **6** to post-consumer plastic mixtures, depolymerization of end-of-life Nylon-6 fishing net was carried out admixed with a PE water bottle cap in a 1:1 mass ratio. This afforded ε-caprolactam in a 95% yield (Table 2, entry 9), while the unreactive PE bottle cap was recovered unchanged, as evidenced by ^{1}H NMR analysis (Figure S26). This result indicates that catalyst **6** is compatible with mixed-plastic scenarios and can be utilized for the separation of end-of-life Nylon-6 from mixed-plastic, yielding the valuable caprolactam monomer.

Achieving Circularity for End-of-Life Fishing nets

To "close the loop" in a fully circular economy for end-of-life Nylon plastics, it was of interest to determine whether the recovered ε-caprolactam could be re-polymerized to pristine Nylon-6. An anionic polymerization procedure was adapted using NaH and N-acetylcaprolactam as polymerization activators at 140 °C.[55] NMR, MALDI-TOF and GPC analyses were used to confirm the structures of these polymers (see Figure S41-S52). First, pristine commercial ε-caprolactam was used to verify the polymerization methodology, and afforded Nylon-6 with a yield of 96.7% and M_n of 31.2 kg mol^{-1}. Next, the recovered ε-caprolactam from the large-scale depolymerization of virgin Nylon-6 powder (Table 1, entry 8) was polymerized using the same procedure, affording new Nylon-6 with a comparable M_n of 23.7 kg mol^{-1} and yield of 98.1%. This result demonstrates that the ε-caprolactam from catalytic Nylon-6 depolymerization can be re-polymerized via the same method. Finally, the isolated ε-caprolactam (recovered from end-of-life fishing net) was subjected to polymerization to generate new Nylon-6 using the same conditions, affording pristine polymer with M_n of 43.6 kg mol^{-1} and yield of 99.3% (Figure 4). Impressively, the upcycled pristine polymer offers superior quality compared to the original fishing net waste (M_n of 21.7 kg mol^{-1}), highlighting the advantages of Nylon chemical recycling through efficient monomer recovery. This experiment effectively closes the loop for an end-of-life Nylon plastic, imbuing new value to abandoned fishing nets, which to the best of our knowledge, is unprecedented.

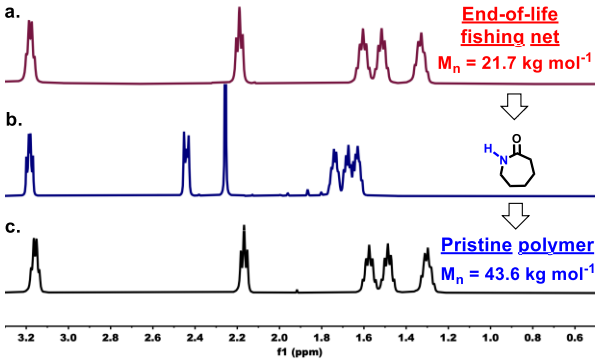

Figure 4. ^{1}H NMR ($CDCl_3$, 500 MHz) spectra of **a**). an end-of-life fishing net; **b**). crude ε-caprolactam product collected from depolymerization of the fishing net; **c**). pristine Nylon-6 obtained from the subsequent re-polymerization.

Experimental Investigation of the Depolymerization Mechanism.

A. Comparing Activity of Catalyst **1** and Catalyst **3**

Catalyst **3** was selected as the most realistic structure to probe the lanthanocene-mediated depolymerization mechanism since it exhibits the highest catalytic activity for powdered virgin Nylon-6. For this Nylon-6 the average number of monomer units in a polymer chain (i.e., degree of polymerization, DP) is estimated to be ~130 (calculated from M_n = 14,800 g mol^{-1} and the repeat unit mass, 113 g mol^{-1}). For 1 mol% catalyst loading, the estimated polymer chain: La ratio is ≈ 1:1.3, indicating more than 1 La catalyst molecule per 1 polymer chain with no interchain La "hopping" required to consume 1 Nylon-6 chain. This agrees with the experimental results (Table 1, entries 1 and 4) that both catalyst **1** and catalyst **3** provide reasonable catalytic activities and yields at 1 mol% catalyst loading (yields of 69% and 91%, respectively). In contrast, for a low catalyst loading of 0.2 mol%, the calculated polymer chain: La ratio is ≈ 5:1. In this scenario, the La catalyst must be able to "hop" between polymer chains to achieve high depolymerization conversions. Under these conditions, catalyst **1** only provides a 5.6% ε-caprolactam yield (Table 1, entry 2), while the performance of catalyst **3** is barely impacted from the lower loading (Table 1, entries 6-8, 11).

To gain further insights into the greater performance of catalyst **3** *vs* **1**, additional experiments were carried out. This laboratory previously reported that for the depolymerization of Nylon-6 using catalyst **1**, all threeTMS_2N- ligands participate in the Nylon activation step (2.5 equiv. of

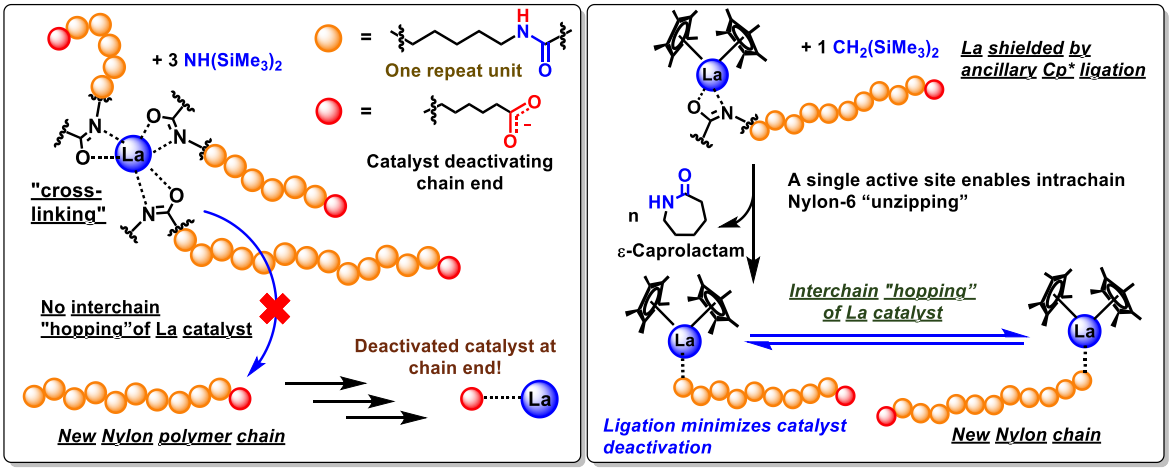

Figure 5. Illustration of different proposed depolymerization pathways for catalyst **1** (left) and catalyst **3** (right). Dashed lines between La and polymer chains portray the interaction and binding between the metal ion and amide bonds of Nylon-6.

TMS_2NH are released at the onset of reaction).[30] Based on this finding, it seems unlikely that catalyst **1** can readily interchain "hop" following the consumption/deconstruction of a polymer chain, reflecting the aforementioned La-polymer macromolecule cross-linkages arising from the homo-

To validate this mechanistic hypothesis, ^{1}H NMR analysis at the onset of the depolymerization process was performed (see SI Section 4 for the full spectrum analysis). The data reveal gradual protonolysis of the La-$CH(TMS)_2$ linkage with ~95% of the expected $CH_2(TMS)_2$ obtained.

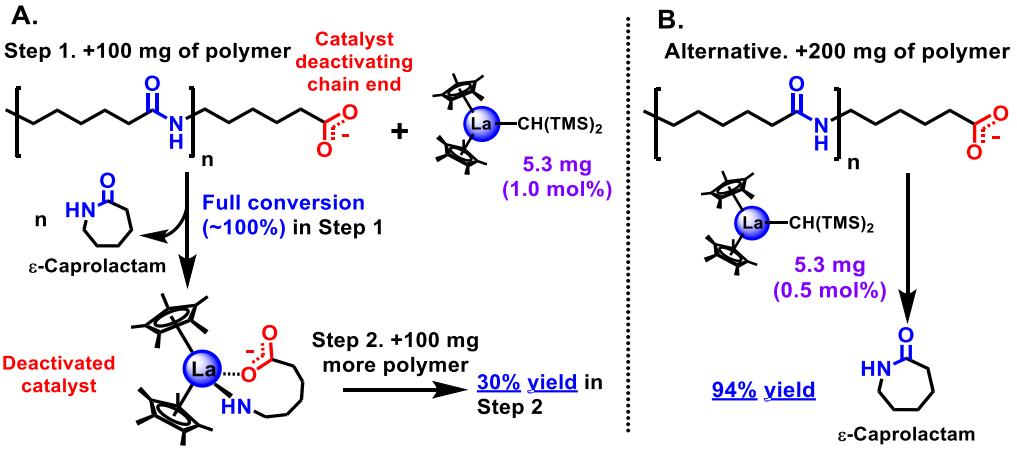

Figure 6. Experiments to define catalyst deactivation by chain ends of Nylon-6. See Section 5 of the SI for experimental details.

leptic tris-amido structure (Figure 5, left). Instead, deactivation of catalyst **1** by a carboxylate chain end (see below for details) can occur. In contrast, the non-dissociable Cp* ligands of catalyst **3** can sterically shield the La center and likely hinder the undesired cross-linking and catalyst immobilization. Importantly, this may promote effective interchain-hopping by catalyst **3** when low catalyst loadings are employed (supported by DFT calculations, *vide infra*).

Only trace amounts (<5% yield) of a Cp*H protonolysis product are detected, in accord with the stability the Ln-Cp* ligation. Here, we propose a plausible process for the deconstruction of Nylon-6 via intrachain "unzipping" by catalyst **3** (Figure 5, right). Unlike catalyst **1**, deactivation of catalyst **3** at the polymer chain ends can be minimized by effective interchain "hopping", achieving high-yield depolymerization a low catalyst loadings.

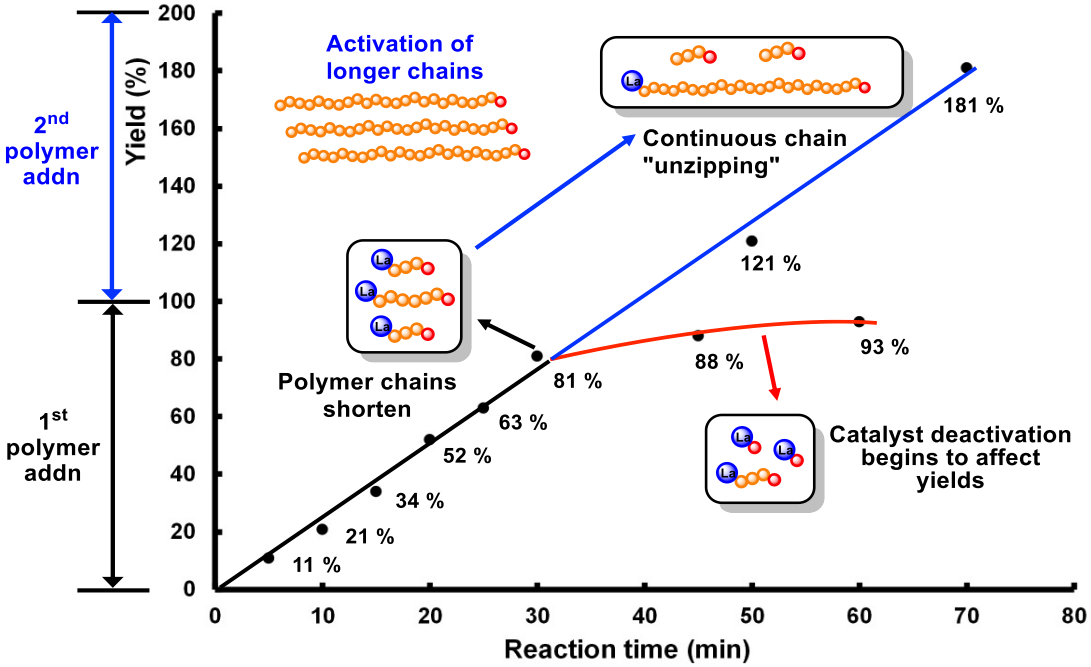

Figure 7. Kinetic studies to characterize Nylon-6 depolymerization pathway. Reaction conditions for the first batch of polymer: 0.2 mol% of catalyst **3**, 240 °C, 100 mg of Nylon-6. Yields calculated for the first batch of polymer. Black and red traces represent the kinetic profile of the first polymer batch. The blue line represents continuous linear growth of yield when second batch of polymer (100 mg) is added at 30 min.

B. Chain-End Catalyst Deactivation and Kinetic Analysis

Next, catalyst deactivation at the polymer chain ends was probed experimentally. After reaching full depolymerization conversions, the catalytic species is likely to reach the carboxylate chain ends to form a stable, inactive complex (see Figure 6A for a plausible deactivated catalyst structure). Under this hypothesis, following the consumption of an initial polymer batch, the residual reaction mixture should exhibit much poorer catalytic depolymerization activity for a second polymer batch. As depicted in Figure 6A, the catalyst deactivation process is supported by this "stepwise" polymer addition test. To ensure a full depolymerization conversion for the first batch of polymer, the reaction conditions employed in Table 1, entry 5, were adopted. The depolymerization rate of the second polymer batch is found to be substantially lower, providing only a 30% yield in the second run. Conversely, depolymerization of a combined 200 mg polymer sample, added in a non-stepwise manner, under the same catalytic conditions, achieves superior reactivity (94% yield; Figure 6B).

To probe the kinetic profile of **3**-mediated depolymerization, the ε-caprolactam yield is plotted *vs* the reaction time (Figure 7) using a low catalyst loading (0.2 mol%). A linear increase in ε-caprolactam yield is evident over the first 30 min (up to 81% yield; Figure 7, black line), followed by a saturation of yield in the later stages of the reaction (30-60 mins from 81% to 93% yield; Figure 7, red curve). Since catalyst deactivation can occur at the carboxylate group chain ends, we suggest that the declining reaction rate after 30 min occurs as the depolymerization of shorter polymer chains is completed. To test this hypothesis, two depolymerization reactions were carried out under the same conditions and halted at 30 min to avoid reaching full conversion and catalyst deactivation. To these reaction residues, were added the same amounts of pristine Nylon-6 without quenching any reaction intermediates, and the mixtures were allowed to react for another 20 and 40 min,

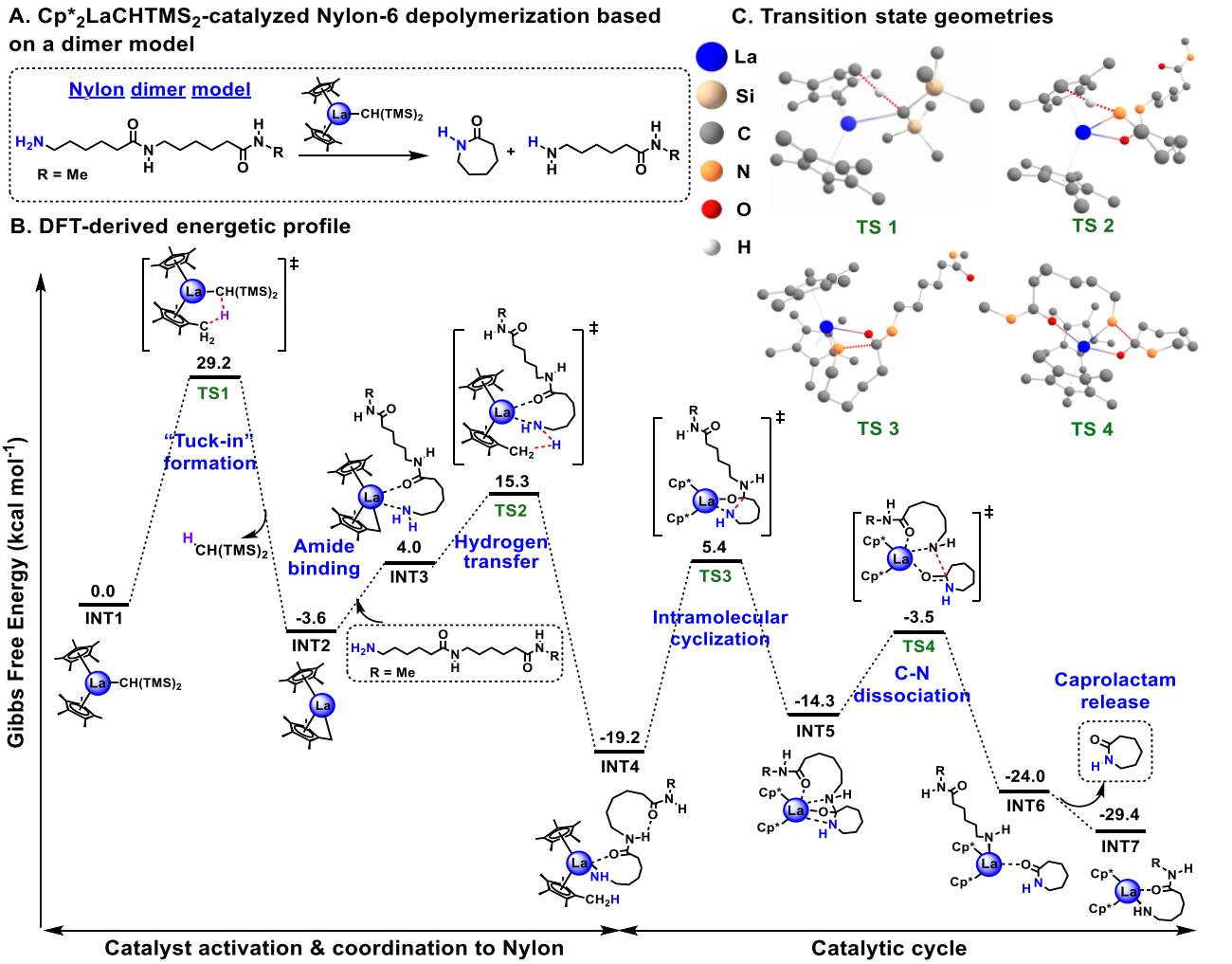

Figure 8. DFT analysis for the depolymerization of Nylon-6 using a dimer model. **A**) Computed Nylon dimer model reaction. **B**) DFT-derived energetic (Gibbs free-energy) profile in a solution phase (kcal mol^{-1}). **C**) Computed transition state geometries. Reaction pathways are highlighted in red dashed lines. Hydrogen atoms that are not involved in the reactions are deleted for clarity.

respectively (see SI for experimental details). The results show a continuing linear growth of ε-caprolactam yield (Figure 7, blue line) without saturation after 30 min, in direct contrast to the initial kinetic trend (red curve). In this case, the addition of long polymer chains at 30 min allows the La to "hop" from the shorter chains to longer chains before catalyst deactivation at the chain ends. These model studies also suggest the potential for ultra-low catalyst loading for Nylon-6 depolymerization by continuous feed strategies. As a demonstration of this concept, the experiment presented above effectively decreases the catalyst loading of **3** from 0.2 mol% to 0.1 mol% through the addition of new polymers before reaching full depolymerization conversion.

DFT Analysis.

To further probe the mechanism of lanthanocene-mediated depolymerization, a detailed Gibbs free energy profile was computed for catalyst **3** (Figure 8), as it provides the highest catalytic activity and is used for the aforementioned experimental mechanistic studies. DFT calculations were performed using a Nylon-6 dimer model (Figure 8A) to accurately simulate the coordination of the electrophilic La^{3+} center to an actual polymer. The initial step involves a proton abstraction on the Cp* ligand via intramolecular C-H activation to produce quantitative evolution of $CH_2(TMS)_2$ (supported by ^1H NMR experiments, see above and Section 4 of the SI for discussion) and a lanthanocene "tuck-in" structure[56] (**INT2**). Note that this computed pre-catalyst thermolysis process is in good agreement with a previous report by our laboratory,[34] in which the thermolysis product of catalyst **3** is shown to exhibit an indistinguishable catalytic activity *vs* that of the original catalyst. This step is slightly exergonic (ΔG = -3.6 kcal mol^{-1}) with a barrier of $\Delta G^{\ddagger}$ = 29.2 kcal mol^{-1} (**TS1**), and is estimated by computational modeling to be a rapid process (completed in only 2s, see Figure S54 for details). In contrast, this activation step for catalyst **2** with a less reactive ligand (-NTMS) is calculated to be unfavorable (ΔG = 19.2 kcal mol^{-1}) with a much higher barrier ($\Delta G^{\ddagger}$ = 39.5 kcal mol^{-1}) to yield **INT2**, in accord with its low activity (Figure S55). Next, coordination of La to the oxygen atom of an amide group in an endergonic step (ΔG = 7.6 kcal mol^{-1}) yields **INT3**, which is stabilized by the intramolecular coordination to the -NH_2 chain end. The tuck-in moiety reverts to the initial Cp*$_2$-La structure in a favorable exergonic H-transfer step from the terminal amine (ΔG = -23.2 kcal mol^{-1}; a barrier of $\Delta G^{\ddagger}$ = 11.3 kcal mol^{-1}) to yield **INT4**. This step is also confirmed by a Cp*$_2$Ln-catalyzed hydroamination study in which the rapid protonolysis of **INT2** by amine substrates was observed experimentally.[34] Once **INT4** enters the catalytic cycle (Figure 9), an intramolecular cyclization yields **INT5** in a slightly endergonic step (ΔG = 4.9 kcal mol^{-1}) with a barrier of $\Delta G^{\ddagger}$ = 24.6 kcal mol^{-1} (**TS3**), which is the rate-determining step in the cycle. The importance of utilizing a dimer model is highlighted by mimicking a polymer chain to provide an extra coordination from an adjacent amide, which stabilizes **INT5** by 2.3 kcal mol^{-1} (Figure S56) and more accurately depicts a La-polymer binding scenario. Moreover, the barrier for the less active Y analogue (catalyst **5**) of this rate-determining step (**TS3**) is computed to be 3.3 kcal mol^{-1} higher than for catalyst **3** (Figure S57), in excellent agreement with experimental results. Next, **INT6** is formed via an exergonic (ΔG = -9.7 kcal mol^{-1}) C-N dissociation step, which has a barrier of $\Delta G^{\ddagger}$ = 10.8 kcal mol^{-1} (**TS4**). Lastly, ε-caprolactam is released in a slightly exergonic step (ΔG = -5.4 kcal mol^{-1}), yielding **INT7** with a second Nylon-6 monomer coordinated to the La center to complete the catalytic cycle (also see Figure 9).

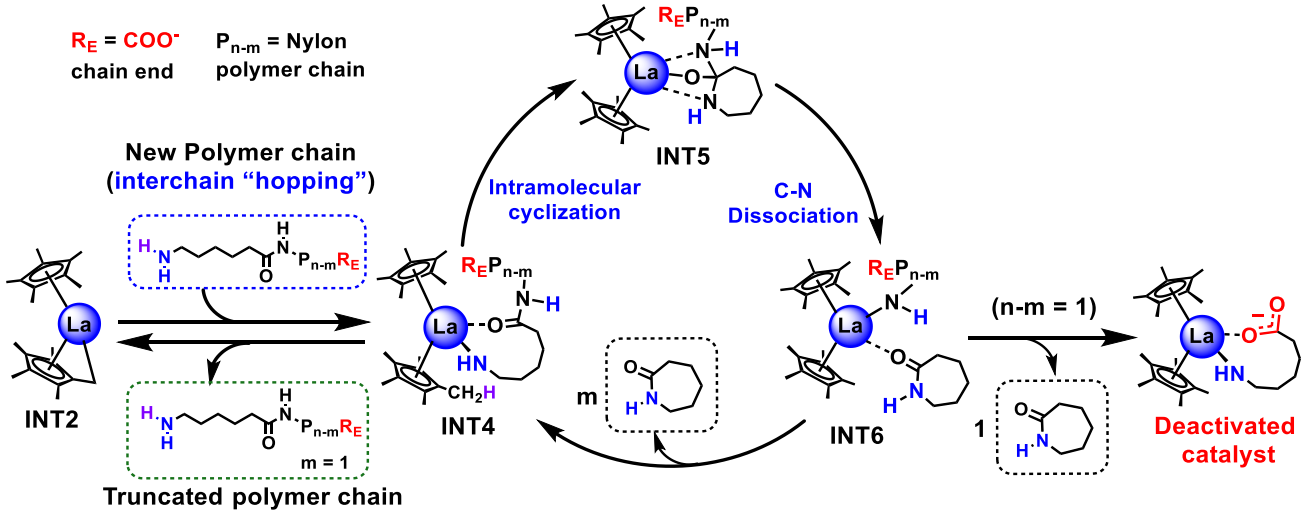

Figure 9. Proposed catalytic cycle for the depolymerization of Nylon-6. Schematic illustrations of the interchain "hopping" and end-chain catalytic deactivation mechanisms are included. A counter cation is not included in the deactivated catalyst structure for clarity.

Next, the interchain "hopping" mechanism was investigated to support the **3**-mediated depolymerization pathway proposed in Figure 5. Besides continuing the catalytic cycle with the coordinated polymer chain, another possible pathway for **INT4** is proposed to undergo a polymer-polymer

exchange via **INT2** in reversable steps (Figure 9). To evaluate this mechanism, a concentration modeling was performed by computing the interchain "hopping" of catalyst **3** between two Nylon dimer models (Figure S58). Simulation shows La hops within seconds at 240 °C, and an equilibrium is reached in only 3 min to allow rapid Nylon interchain exchange. Chain-end catalyst deactivation (Figure 9, n-m=1) was also examined computationally (Figure S59). In a computed structure for the deactivated catalyst, La is coordinated to the carboxylate chain end and a terminal primary amine. This complex is found to be unfavorable (ΔG = 1.5 kcal mol^{-1}) for hopping to a new polymer chain (simulated by a dimer model) and regenerating the active species **INT4**, which validates its deactivation and is in good agreement with experiment (Figure 6).

CONCLUSIONS

This study demonstrates rational catalyst design as a promising pathway to realize rapid and selective Nylon plastics deconstruction. By fine-tuning the catalyst structures, we investigated a series of lanthanocenes and identified extremely efficient catalysts for the chemical recycling of Nylon-6 in a solventless, scalable process. For example, catalyst **3** is a highly effective catalyst for the depolymerization of powdered Nylon-6 (affording up to >99 % yield of the monomer ε-caprolactam) at temperatures as low as 220 °C and catalyst loadings as low as 0.2 mol%. These conditions, to the best of our knowledge, are the mildest to date for Nylon-6 depolymerization to ε-caprolactam in the peer-reviewed literature. For the more challenging deconstruction of waste Nylon-6 commodity products, *ansa*-yttrocene complex **6** was found to efficiently depolymerize a variety of end-of-life Nylon plastics, including fishing nets, carpets, clothing, gloves, as well as in a mix-plastic case. Moreover, the ε-caprolactam collected from these end-of-life Nylons was demonstrated to be re-polymerizable to pristine Nylon-6 with comparable or higher quality, "closing the loop" and achieving model circularity for Nylon plastics. Mechanistic experiments supported by DFT calculations show that the implementation of non-dissociable π-ancillary ligands in these effective catalysts is crucial in sterically shielding the metal center to allow intrachain "unzipping" and effective interchain "hopping" processes, minimizing catalyst crosslinkages and chain-end deactivations.

EXPERIMENTAL SECTION

Materials and Methods. La^{NTMS} (**1**) was obtained from Strem Chemicals. $Cp^*_2LaN(TMS)_2$ (**2**), $Cp^*_2LaCH(TMS)_2$ (**3**), $Cp^*_2LuCH(TMS)_2$ (**4**), $Cp^*_2YCH(TMS)_2$ (**5**), $Me_2SiCp''_2YCH(TMS)_2$ (**6**) were synthesized according to published reports.[33,48,57] All polymers were washed with 1 M KOH solution overnight,[30] filtered, washed with deionized H_2O, and dried under a high vacuum at 100 °C for at least 24 h prior to use. Pristine Nylon-6 powder with a mean particle size of 15-20 μm and a molecular mass (M_n) of 14,800 g/mol (as determined by GPC) was obtained from Goodfellow Inc. All manipulations in catalyst synthesis were carried out with the exclusion of O_2 and moisture in oven-dried Schlenk-type glassware on either a dual-manifold Schlenk line, interfaced to a high-vacuum manifold (10^{-6} Torr), or in an Argon-filled MBraun glovebox with a high-capacity recirculatory (< 1 ppm O_2). All depolymerization reactions were assembled by mixing the polymer and the appropriate catalyst in a Argon-filled MBraun glovebox in cylindrical 50 mL Schlenk tubes. Heating was supplied by a customized aluminum heating block with a fitted hole for the Schlenk tubes. See Figure S1 for a typical depolymerization setup.

Physical and Analytical Methods. NMR spectra were recorded on a Varian Bruker Advance III HD system equipped with a TXO Prodigy probe (500 MHz) spectrometer. Chemical shifts (δ) for ^1H NMR are referenced to the internal solvent. NMR spectra of re-polymerized Nylon-6 were measured by dissolving the polymer samples in trifluoroethanol (TFE) and a few drops of $CDCl_3$. Mass Spectrum data was collected on Bruker Rapiflex MALDI-TOF, using FlexControl data acquisition software and processed using FlexAnalysis software for data analysis. Polymer samples for MALDI-TOF were analyses dissolved in hexafluoroisopropanol (HFIP) at a concentration of 5 mg/mL. The matrix used was 2-(4-hydroxyphenylazo)-benzoic acid (HABA). The layered sample preparation technique was used in which 2 μL of saturated HABA matrix in HFIP solution was applied to the sample target, dried in air, covered with a 2 μL-layer of sample solution, dried in air, and followed by a final layer of matrix solution. GPC was used to analyze the number avarage molecular weight (M_n), weight average molecular weight (Mw), and molecular weight dispersity indices ($Đ$) of Nylon-6 samples. An Agilent Infinity II 1260 high-performance liquid chromatography (HPLC) system was coupled with Wyatt Mini-DAWN TREOS Multi-Angle Light Scattering (MALS, 3 angles) and Optilab T-Rex Refractive Index (RI, 658 nm) detectors. Polymer concentrations of 5.0 ± 0.05 mg/mL in hexafluoroisopropanol (HFIP, ChemImpex) amended with 20mM sodium trifluoroacetate (NaTFAc, Sigma Aldrich) were prepared by dissolving each polymer at room temperature on a shaker plate, followed by filtration through a 0.2 μm syringe filter. Samples were injected at a volume of 100 μL into the system at a flow rate of 0.35 mL/min (HFIP with 20 mM NaTFA) through 3 Plgel-HFIP columns in series with a guard column at 40 °C. Astra 7 software was used to determine absolute M_n, M_w, and dispersity ($Đ$, M_w/M_n) using a d*n*/d*c* values calculated by assuming 100% mass recovery using the known concentration of each sample. Polymethyl methacrylate and polyethylene terephthalate standards were used to check instrumentation and validate results.

General Procedure for Depolymerization Reactions. In a glove box, a 50 mL oven-dried Schlenk tube was charged with a magnetic stir bar, pristine Nylon-6 fine powder (or post-consumer Nylon product), and finely ground catalyst. The vessel was sealed tightly, and the polymer and catalyst were thoroughly mixed by stirring at room temperature for approximately 5 min. The Schlenk tube was then evacuated to 10^{-3} Torr, sealed, and heated to the specified temperature

with slow magnetic stirring (50-100 rpm) for the specified time. Reaction time was recorded starting 2.5 min after the reaction tube was placed in the heating block, since it takes an average of 2.5 min for the reaction to reach the depolymerization temperature and the polymer to begin melting. During the reaction, the ε-caprolactam product sublimes from the hot reaction zone and deposit as a crystalline layer on the cold wall of the reactor. After cooling to room temperature, the soluble part of the reaction mixture was dissolved in 3-4 mL of deuterated solvent, and mesitylene was added as an internal standard. A sample of this solution was withdrawn for NMR analysis. Yields were determined by ^{1}H NMR, comparing the signal integrals of ε-caprolactam and mesitylene.

Computational Details. All quantum chemical calculations were performed using the ORCA 5.0.3 package.[58,59] The geometric optimizations were calculated with the hybrid functional of PBE0[60,61] with the Def2-SVP basis set of the Ahlrichs group[62,63] along with dispersion corrections quantified by the DFT-D3[64] method with Grimme's Becke-Johnson (BJ) damping.[65] Frequency calculations were performed at the same level of theory, all minima were confirmed to have zero imaginary frequency modes, while transition states showed exactly one negative frequency mode. The single-point calculations were performed at a higher level of theory, PBE0-D3/Def2-TZVP, using the solvation model based on density (SMD).[66] N-methylformamide was chosen as the solvent since it represents the solvent environment of the melted Nylon-6 polymer. In addition, to accelerate the DFT calculations, resolution of identity approximation (RI)[67] was used for the Coulomb integrals, and efficiently computed the exchange terms using the "chain-of-spheres" (COSX)[68] approximation with the def2/J auxiliary basis set. The visualization software used was Chemcraft.[69] Three different configurations for the coordination of Nylon-6 dimer model to catalysts were considered, namely "Linear", "Crest" (conformer searched using the CREST package[70]) and "Curve", see details in the SI. Shermo[71] was used for the Gibbs free energy files based on the frequency and single point energy calculations with Grimme's entropy interpolation[72] for quasi rigid-rotor harmonic oscillator (QRRHO) approximation. All thermodynamic values are reported at 1 atm and at 240 °C with a concentration of 1 M to capture the variation of Gibbs free energy due to concentration change from the gas phase (1 atm) to the liquid phase standard state (1 M). Concentration modeling was performed by Concvar[73] based on the calculated Gibbs free energy profile.

ASSOCIATED CONTENT

Supporting Information

The Supporting Information is available free of charge on the ACS Publications website.

Experimental procedures, spectra for products, supplementary figures (PDF)

Optimized DFT structures and coordinates of all computed structures (ZIP file)

AUTHOR INFORMATION

Corresponding Authors

Linda J. Broadbelt − Department of Chemical and Biological Engineering, Northwestern University, Evanston, Illinois 60208-3113, United States; orcid.org/0000-0003-4253-592X; Email: broadbelt@northwestern.edu

Yosi Kratish − Department of Chemistry, Northwestern University, Evanston, Illinois 60208-3113, United States; orcid.org/0000-0001-5279-0268; Email: yosi.kratish@northwestern.edu

Tobin J. Marks − Department of Chemistry, Northwestern University, Evanston, Illinois 60208-3113, United States; orcid.org/0000-0001-8771-0141; Email: t-marks@northwestern.edu

Authors

Liwei Ye − Department of Chemistry, Northwestern University, Evanston, Illinois 60208-3113, United States; orcid.org/0000-0002-5878-5029

Xiaoyang Liu − Department of Chemical and Biological Engineering, Northwestern University, Evanston, Illinois 60208-3113, United States; orcid.org/0000-0002-8172-6756

Kristen Beckett − Department of Chemistry, Northwestern University, Evanston, Illinois 60208-3113, United States

Jacob O. Rothbaum − Department of Chemistry, Northwestern University, Evanston, Illinois 60208-3113, United States; orcid.org/0000-0002-4337-2184

Clarissa Lincoln – Renewable Resources and Enabling Sciences Center, National Renewable Energy Laboratory, Golden, CO 80401, United States

Notes

The authors declare no competing financial interest.

ACKNOWLEDGMENT

The support of RePLACE (Redesigning Polymers to Leverage A Circular Economy), funded by the Office of Science of the U.S. Department of Energy via award no. DR-SC0022290 (T.J.M., L.Y., K.B., L.J.B, X.L.) is gratefully acknowledged. Y.K. acknowledges support by the Office of Basic Energy Sciences, U.S. Department of Energy (DE-FG02-03ER15457) to the Institute for Catalysis in Energy Processes (ICEP) at Northwestern University. J.O.R. acknowledges support from NSF CAT Program grant CHE-1856619 and Northwestern for Academy Fellowship. This work made use of the IMSERC NMR facility at Northwestern University, supported by NSF (CHE-1048773). This work used Expanse at San Diego Supercomputer Center through allocation CTS120055 from the Advanced Cyberinfrastructure Coordination Ecosystem: Services & Support (ACCESS) program, which is supported by National Science Foundation grants # OAC-2138259, # OAC-2138286, # OAC-2138307, # OAC-2137603, and # OAC-2138296. This work was authored in

part by the National Renewable Energy Laboratory, operated by Alliance for Sustainable Energy, LLC, for the U.S. Department of Energy (DOE) under Contract No. DE-AC36-08GO28308. Funding provided by the US Department of Energy, Office of Energy Efficiency and Renewable Energy, Advanced Manufacturing Office (AMO) and Bioenergy Technologies Office (BETO). This work was performed as part of the Bio-Optimized Technologies to keep Thermoplastics out of Landfills and the Environment (BOTTLE) Consortium and was supported by AMO and BETO under contract no. DE-AC36-08GO28308 with the National Renewable Energy Laboratory(NREL), operated by Alliance for Sustainable Energy, LLC. The views expressed in the article do not necessarily represent the views of the DOE or the U.S. Government. The U.S. Government retains and the publisher, by accepting the article for publication, acknowledges that the U.S. Government retains a nonexclusive, paid-up, irrevocable, worldwide license to publish or reproduce the published form of this work, or allow others to do so, for U.S. Government purposes.

REFERENCES

(1) Jehanno, C.; Pérez-Madrigal, M. M.; Demarteau, J.; Sardon, H.; Dove, A. P. Organocatalysis for Depolymerisation. *Polym. Chem.* **2019**, *10* (2), 172–186. https://doi.org/10.1039/C8PY01284A.

(2) Coates, G. W.; Getzler, Y. D. Y. L. Chemical Recycling to Monomer for an Ideal, Circular Polymer Economy. *Nat Rev Mater* **2020**, *5* (7), 501–516. https://doi.org/10.1038/s41578-020-0190-4.

(3) Chu, M.; Liu, Y.; Lou, X.; Zhang, Q.; Chen, J. Rational Design of Chemical Catalysis for Plastic Recycling. *ACS Catal.* **2022**, *12* (8), 4659–4679. https://doi.org/10.1021/acscatal.2c01286.

(4) Bergmann, M.; Almroth, B. C.; Brander, S. M.; Dey, T.; Green, D. S.; Gundogdu, S.; Krieger, A.; Wagner, M.; Walker, T. R. A Global Plastic Treaty Must Cap Production. *Science* **2022**, *376* (6592), 469–470. https://doi.org/10.1126/science.abq0082.

(5) Law, K. L.; Narayan, R. Reducing Environmental Plastic Pollution by Designing Polymer Materials for Managed End-of-Life. *Nat Rev Mater* **2021**, *7* (2), 104–116. https://doi.org/10.1038/s41578-021-00382-0.

(6) Geyer, R.; Jambeck, J. R.; Law, K. L. Production, Use, and Fate of All Plastics Ever Made. *Sci. Adv.* **2017**, *3* (7), e1700782. https://doi.org/10.1126/sciadv.1700782.

(7) *Global Nylon Market Analysis and Outlook 2020-2027 - Nylon 6 Volumes Will Reach 5.3 Million Tons by 2027, Despite COVID-19 - ResearchAndMarkets.com*. https://www.businesswire.com/news/home/20200730005398/en/Global-Nylon-Market-Analysis-and-Outlook-2020-2027---Nylon-6-Volumes-Will-Reach-5.3-Million-Tons-by-2027-Despite-COVID-19---ResearchAndMarkets.com (accessed 2023-01-19).

(8) Hole, G.; Hole, A. S. Improving Recycling of Textiles Based on Lessons from Policies for Other Recyclable Materials: A Minireview. *Sustainable Production and Consumption* **2020**, *23*, 42–51. https://doi.org/10.1016/j.spc.2020.04.005.

(9) Agenda, I. The New Plastics Economy Rethinking the Future of Plastics; 2016; p 36.

(10) Macfadyen, G.; Huntington, T.; Cappell, R. Abandoned, Lost or Otherwise Discarded Fishing Gear. *UNEP Regional Seas Reports and Studies* **2009**, *185*.

(11) Chhabra, E. Recycling Nylon Is Good for the Planet – so Why Don't More Companies Do It? *The Guardian*. May 18, 2016. https://www.theguardian.com/sustainable-business/2016/may/18/recycling-nylon-bureo-patagonia-sustainable-clothing (accessed 2022-12-12).

(12) Lebreton, L.; Slat, B.; Ferrari, F.; Sainte-Rose, B.; Aitken, J.; Marthouse, R.; Hajbane, S.; Cunsolo, S.; Schwarz, A.; Levivier, A.; Noble, K.; Debeljak, P.; Maral, H.; Schoeneich-Argent, R.; Brambini, R.; Reisser, J. Evidence That the Great Pacific Garbage Patch Is Rapidly Accumulating Plastic. *Sci Rep* **2018**, *8* (1), 4666. https://doi.org/10.1038/s41598-018-22939-w.

(13) Nelms, S. E.; Barnett, J.; Brownlow, A.; Davison, N. J.; Deaville, R.; Galloway, T. S.; Lindeque, P. K.; Santillo, D.; Godley, B. J. Microplastics in Marine Mammals Stranded around the British Coast: Ubiquitous but Transitory? *Sci Rep* **2019**, *9* (1), 1075. https://doi.org/10.1038/s41598-018-37428-3.

(14) Matthies, P.; Seydl, W. F. History and Development of Nylon 6. In *High Performance Polymers: Their Origin and Development*; Seymour, R. B., Kirshenbaum, G. S., Eds.; Springer Netherlands: Dordrecht, 1986; pp 39–53. https://doi.org/10.1007/978-94-011-7073-4_4.

(15) *Polyesters and Polyamides*; Deopura, B. L., Alagirusamy, R., Textile Institute, Eds.; Woodhead Publishing in textiles; CRC Press: Boca Raton, Fla., 2008.

(16) *Nylon Market Size, Share, Report | Global Industry Trends, 2029*. https://www.fortunebusinessinsights.com/nylon-market-102007 (accessed 2022-12-11).

(17) *Nylon Market Size, Share & Trends Report, 2022-2030*. https://www.grandviewresearch.com/industry-analysis/nylon-6-6-market (accessed 2022-12-11).

(18) Cywar, R. M.; Rorrer, N. A.; Mayes, H. B.; Maurya, A. K.; Tassone, C. J.; Beckham, G. T.; Chen, E. Y.-X. Redesigned Hybrid Nylons with Optical Clarity and Chemical Recyclability. *J. Am. Chem. Soc.* **2022**, *144* (12), 5366–5376. https://doi.org/10.1021/jacs.1c12611.

(19) Braun, M.; Levy, A. B.; Sifniades, S. Recycling Nylon 6 Carpet to Caprolactam. *Polymer-Plastics Technology and Engineering* **1999**, *38* (3), 471–484. https://doi.org/10.1080/03602559909351594.

(20) Alberti, C.; Figueira, R.; Hofmann, M.; Koschke, S.; Enthaler, S. Chemical Recycling of End-of-Life Polyamide 6 via Ring Closing Depolymerization. *ChemistrySelect* **2019**, *4* (43), 12638–12642. https://doi.org/10.1002/slct.201903970.

(21) Nielsen, M.; Jurasek, P.; Hayashi, J.; Furimsky, E. Formation of Toxic Gases during Pyrolysis of Polyacrylonitrile and Nylons. *Journal of Analytical and Applied Pyrolysis* **1995**, *35* (1), 43–51. https://doi.org/10.1016/0165-2370(95)00898-O.

(22) Lozano-González, Ma. J.; Rodriguez-Hernandez, Ma. T.; Gonzalez-De Los Santos, E. A.; Villalpando-Olmos, J. Physical-Mechanical Properties and Morphological Study on Nylon-6 Recycling by Injection Molding. *J. Appl. Polym. Sci.* **2000**, *76* (6), 851–858. https://doi.org/10.1002/(SICI)1097-4628(20000509)76:6<851::AID-APP11>3.0.CO;2-D.

(23) *Ullmann's Encyclopedia of Industrial Chemistry*, 1st ed.; Wiley, 2000. https://doi.org/10.1002/14356007.
(24) Bradford, S.; Rupf, R.; Stucki, M. Climbing Ropes—Environmental Hotspots in Their Life Cycle and Potentials for Optimization. *Sustainability* **2021**, *13* (2), 707. https://doi.org/10.3390/su13020707.
(25) Mihut, C.; Captain, D. K.; Gadala-Maria, F.; Amiridis, M. D. Review: Recycling of Nylon from Carpet Waste. *Polymer Engineering & Science* **2001**, *41* (9), 1457–1470. https://doi.org/10.1002/pen.10845.
(26) Kamimura, A.; Yamamoto, S. An Efficient Method To Depolymerize Polyamide Plastics: A New Use of Ionic Liquids. *Org. Lett.* **2007**, *9* (13), 2533–2535. https://doi.org/10.1021/ol070886c.
(27) Yamamoto, S.; Kamimura, A. Preparation of Novel Functionalized Ammonium Salts That Effectively Catalyze Depolymerization of Nylon-6 in Ionic Liquids. *Chem. Lett.* **2009**, *38* (11), 1016–1017. https://doi.org/10.1246/cl.2009.1016.
(28) Kamimura, A.; Shiramatsu, Y.; Kawamoto, T. Depolymerization of Polyamide 6 in Hydrophilic Ionic Liquids. *Green Energy & Environment* **2019**, *4* (2), 166–170. https://doi.org/10.1016/j.gee.2019.01.002.
(29) Kumar, A.; von Wolff, N.; Rauch, M.; Zou, Y.-Q.; Shmul, G.; Ben-David, Y.; Leitus, G.; Avram, L.; Milstein, D. Hydrogenative Depolymerization of Nylons. *J. Am. Chem. Soc.* **2020**, *142* (33), 14267–14275. https://doi.org/10.1021/jacs.0c05675.
(30) Wursthorn, L.; Beckett, K.; Rothbaum, J. O.; Cywar, R. M.; Lincoln, C.; Kratish, Y.; Marks, T. J. Selective Lanthanide-Organic Catalyzed Depolymerization of Nylon-6 to E-Caprolactam. *Angew Chem Int Ed* **2022**. https://doi.org/10.1002/anie.202212543.
(31) Bradley, D. C.; Ghotra, J. S.; Hart, F. A. Low Co-Ordination Numbers in Lanthanide and Actinide Compounds. Part I. The Preparation and Characterization of Tris{bis(Trimethylsilyl)-Amido}lanthanides. *J. Chem. Soc., Dalton Trans.* **1973**, No. 10, 1021. https://doi.org/10.1039/dt9730001021.
(32) Jehanno, C.; Alty, J. W.; Roosen, M.; De Meester, S.; Dove, A. P.; Chen, E. Y.-X.; Leibfarth, F. A.; Sardon, H. Critical Advances and Future Opportunities in Upcycling Commodity Polymers. *Nature* **2022**, *603* (7903), 803–814. https://doi.org/10.1038/s41586-021-04350-0.
(33) Jeske, G.; Lauke, H.; Mauermann, H.; Swepston, P. N.; Schumann, H.; Marks, T. J. Highly Reactive Organolanthanides. Systematic Routes to and Olefin Chemistry of Early and Late Bis(Pentamethylcyclopentadienyl) 4f Hydrocarbyl and Hydride Complexes. *J. Am. Chem. Soc.* **1985**, *107* (26), 8091–8103. https://doi.org/10.1021/ja00312a050.
(34) Ryu, J.-S.; Marks, T. J.; McDonald, F. E. Organolanthanide-Catalyzed Intramolecular Hydroamination/Cyclization/Bicyclization of Sterically Encumbered Substrates. Scope, Selectivity, and Catalyst Thermal Stability for Amine-Tethered Unactivated 1,2-Disubstituted Alkenes. *J. Org. Chem.* **2004**, *69* (4), 1038–1052. https://doi.org/10.1021/jo035417c.
(35) Hong, S.; Marks, T. J. Organolanthanide-Catalyzed Hydroamination. *Acc. Chem. Res.* **2004**, *37* (9), 673–686. https://doi.org/10.1021/ar040051r.
(36) Kosloski-Oh, S. C.; Wood, Z. A.; Manjarrez, Y.; de los Rios, J. P.; Fieser, M. E. Catalytic Methods for Chemical Recycling or Upcycling of Commercial Polymers. *Mater. Horiz.* **2021**, *8* (4), 1084–1129. https://doi.org/10.1039/D0MH01286F.
(37) Matthies, P.; Seydl, W. F. History and Development of Nylon 6. In *High Performance Polymers: Their Origin and Development*; Seymour, R. B., Kirshenbaum, G. S., Eds.; Springer Netherlands: Dordrecht, 1986; pp 39–53. https://doi.org/10.1007/978-94-011-7073-4_4.
(38) Rothbaum, J. O.; Motta, A.; Kratish, Y.; Marks, T. J. Chemodivergent Organolanthanide-Catalyzed C–H α-Mono-Borylation of Pyridines. *J. Am. Chem. Soc.* **2022**, *144* (37), 17086–17096. https://doi.org/10.1021/jacs.2c06844.
(39) Heyrovska, R. Dependence of Ion–Water Distances on Covalent Radii, Ionic Radii in Water and Distances of Oxygen and Hydrogen of Water from Ion/Water Boundaries. *Chemical Physics Letters* **2006**, *429* (4–6), 600–605. https://doi.org/10.1016/j.cplett.2006.08.073.
(40) Amin, S. B.; Marks, T. J. Versatile Pathways for In Situ Polyolefin Functionalization with Heteroatoms: Catalytic Chain Transfer. *Angew. Chem. Int. Ed.* **2008**, *47* (11), 2006–2025. https://doi.org/10.1002/anie.200703310.
(41) Schock, L. E.; Marks, T. J. Organometallic Thermochemistry. Metal Hydrocarbyl, Hydride, Halide, Carbonyl, Amide, and Alkoxide Bond Enthalpy Relationships and Their Implications in Pentamethylcyclopentadienyl and Cyclopentadienyl Complexes of Zirconium and Hafnium. *J. Am. Chem. Soc.* **1988**, *110* (23), 7701–7715. https://doi.org/10.1021/ja00231a020.
(42) Booij, M.; Meetsma, A.; Teuben, J. H. Ring Hydrogen C-H Activation in Cp*2LnCH(SiMe3)2 (Ln = Yttrium, Lanthanum, Cerium): X-Ray Crystal Structures of [Cp*3(.Mu.3-.Eta.5,.Eta.1,.Eta.1-C5Me3(CH2)2)Ce2]2 and Cp*2CeCH2C6H5. *Organometallics* **1991**, *10* (9), 3246–3252. https://doi.org/10.1021/om00055a048.
(43) *Current prices for rare earths | Institute for Rare Earths and Metals*. Institut für Seltene Erden und strategische Metalle e.V. https://en.institut-seltene-erden.de/aktuelle-preise-von-seltenen-erden/ (accessed 2023-03-21).
(44) Nuss, P.; Eckelman, M. J. Life Cycle Assessment of Metals: A Scientific Synthesis. *PLoS ONE* **2014**, *9* (7), e101298. https://doi.org/10.1371/journal.pone.0101298.
(45) Moreira, A.; Henriques, B.; Leite, C.; Libralato, G.; Pereira, E.; Freitas, R. Potential Impacts of Lanthanum and Yttrium through Embryotoxicity Assays with Crassostrea Gigas. *Ecological Indicators* **2020**, *108*, 105687. https://doi.org/10.1016/j.ecolind.2019.105687.
(46) Li, Y.; Marks, T. J. Diverse Mechanistic Pathways and Selectivities in Organo-f-Element-Catalyzed Hydroamination. Intermolecular Organolanthanide-Catalyzed Alkyne and Alkene Hydroamination. *Organometallics* **1996**, *15* (18), 3770–3772. https://doi.org/10.1021/om960293y.
(47) Arredondo, V. M.; Tian, S.; McDonald, F. E.; Marks, T. J. Organolanthanide-Catalyzed Hydroamination/Cyclization. Efficient Allene-Based Transformations for the Syntheses of Naturally Occurring Alkaloids. *J. Am. Chem. Soc.* **1999**, *121* (15), 3633–3639. https://doi.org/10.1021/ja984305d.
(48) Jeske, G.; Schock, L. E.; Swepston, P. N.; Schumann, H.; Marks, T. J. Highly Reactive Organolanthanides. Synthesis, Chemistry, and Structures of 4f Hydrocarbyls and Hydrides with Chelating Bis(Polymethylcyclopentadienyl) Ligands. *J. Am. Chem. Soc.* **1985**, *107* (26), 8103–8110. https://doi.org/10.1021/ja00312a051.
(49) Green, J. C.; Jardine, C. N. Thermal Stability of Group 6 Bis(Cyclopentadienyl) and Ethylene Bridged

Bis(Cyclopentadienyl) Monocarbonyl Complexes; a Theoretical Study. *J. Chem. Soc., Dalton Trans.* **1999**, No. 21, 3767–3770. https://doi.org/10.1039/a905363h.

(50) Gagne, M. R.; Stern, C. L.; Marks, T. J. Organolanthanide-Catalyzed Hydroamination. A Kinetic, Mechanistic, and Diastereoselectivity Study of the Cyclization of N-Unprotected Amino Olefins. *J. Am. Chem. Soc.* **1992**, *114* (1), 275–294. https://doi.org/10.1021/ja00027a036.

(51) Falivene, L.; Cao, Z.; Petta, A.; Serra, L.; Poater, A.; Oliva, R.; Scarano, V.; Cavallo, L. Towards the Online Computer-Aided Design of Catalytic Pockets. *Nat. Chem.* **2019**, *11* (10), 872–879. https://doi.org/10.1038/s41557-019-0319-5.

(52) *Carpet Product Stewardship | US EPA*. https://archive.epa.gov/wastes/conserve/tools/stewardship/web/html/carpet.html (accessed 2023-01-21).

(53) Ruggeri, C. *The Environmental Impact of Recycling Carpet | Magazine Aquafil Group*. Aquafil. https://www.aquafil.com/magazine/the-environmental-impact-of-recycling-carpet/ (accessed 2023-01-21).

(54) Peng, Y.; Wu, P.; Schartup, A. T.; Zhang, Y. Plastic Waste Release Caused by COVID-19 and Its Fate in the Global Ocean. *Proc. Natl. Acad. Sci. U.S.A.* **2021**, *118* (47), e2111530118. https://doi.org/10.1073/pnas.2111530118.

(55) Tarkin-Tas, E.; Mathias, L. J. Synthesis and Ring-Opening Polymerization of 5-Azepane-2-One Ethylene Ketal: A New Route to Functional Aliphatic Polyamides. *Macromolecules* **2010**, *43* (2), 968–974. https://doi.org/10.1021/ma902233k.

(56) Schock, L. E.; Brock, C. P.; Marks, T. J. Intramolecular Thermolytic Carbon-Hydrogen Activation Processes. Solid-State Structural Characterization of a Mononuclear .Eta.6-Me4C5CH2 Zirconium Complex and a Mechanistic Study of Its Formation from (Me5C5)2Zr(C6H5)2. *Organometallics* **1987**, *6* (2), 232–241. https://doi.org/10.1021/om00145a003.

(57) Den Haan, K. H.; De Boer, J. L.; Teuben, J. H.; Spek, A. L.; Kojic-Prodic, Biserka.; Hays, G. R.; Huis, Rob. Synthesis of Monomeric Permethylyttrocene Derivatives. The Crystal Structures of Cp2*YN(SiMe3)2 and Cp2*YCH(SiMe3)2. *Organometallics* **1986**, *5* (8), 1726–1733. https://doi.org/10.1021/om00139a034.

(58) Neese, F. The ORCA Program System. *WIREs Computational Molecular Science* **2012**, *2* (1), 73–78. https://doi.org/10.1002/wcms.81.

(59) Neese, F.; Wennmohs, F.; Becker, U.; Riplinger, C. The ORCA Quantum Chemistry Program Package. *J. Chem. Phys.* **2020**, *152* (22), 224108. https://doi.org/10.1063/5.0004608.

(60) Perdew, J. P.; Ernzerhof, M.; Burke, K. Rationale for Mixing Exact Exchange with Density Functional Approximations. *J. Chem. Phys.* **1996**, *105* (22), 9982–9985. https://doi.org/10.1063/1.472933.

(61) Adamo, C.; Barone, V. Toward Reliable Density Functional Methods without Adjustable Parameters: The PBE0 Model. *J. Chem. Phys.* **1999**, *110* (13), 6158–6170. https://doi.org/10.1063/1.478522.

(62) Schäfer, A.; Horn, H.; Ahlrichs, R. Fully Optimized Contracted Gaussian Basis Sets for Atoms Li to Kr. *J. Chem. Phys.* **1992**, *97* (4), 2571–2577. https://doi.org/10.1063/1.463096.

(63) Weigend, F.; Ahlrichs, R. Balanced Basis Sets of Split Valence, Triple Zeta Valence and Quadruple Zeta Valence Quality for H to Rn: Design and Assessment of Accuracy. *Physical Chemistry Chemical Physics* **2005**, *7* (18), 3297–3305. https://doi.org/10.1039/B508541A.

(64) Grimme, S.; Antony, J.; Ehrlich, S.; Krieg, H. A Consistent and Accurate Ab Initio Parametrization of Density Functional Dispersion Correction (DFT-D) for the 94 Elements H-Pu. *J. Chem. Phys.* **2010**, *132* (15), 154104. https://doi.org/10.1063/1.3382344.

(65) Grimme, S.; Ehrlich, S.; Goerigk, L. Effect of the Damping Function in Dispersion Corrected Density Functional Theory. *Journal of Computational Chemistry* **2011**, *32* (7), 1456–1465. https://doi.org/10.1002/jcc.21759.

(66) Marenich, A. V.; Cramer, C. J.; Truhlar, D. G. Universal Solvation Model Based on Solute Electron Density and on a Continuum Model of the Solvent Defined by the Bulk Dielectric Constant and Atomic Surface Tensions. *J. Phys. Chem. B* **2009**, *113* (18), 6378–6396. https://doi.org/10.1021/jp810292n.

(67) Weigend, F. Accurate Coulomb-Fitting Basis Sets for H to Rn. *Physical Chemistry Chemical Physics* **2006**, *8* (9), 1057–1065. https://doi.org/10.1039/B515623H.

(68) Neese, F.; Wennmohs, F.; Hansen, A.; Becker, U. Efficient, Approximate and Parallel Hartree–Fock and Hybrid DFT Calculations. A 'Chain-of-Spheres' Algorithm for the Hartree–Fock Exchange. *Chemical Physics* **2009**, *356* (1), 98–109. https://doi.org/10.1016/j.chemphys.2008.10.036.

(69) *Chemcraft - Graphical program for visualization of quantum chemistry computations*. https://www.chemcraftprog.com/ (accessed 2023-04-19).

(70) Pracht, P.; Bohle, F.; Grimme, S. Automated Exploration of the Low-Energy Chemical Space with Fast Quantum Chemical Methods. *Phys. Chem. Chem. Phys.* **2020**, *22* (14), 7169–7192. https://doi.org/10.1039/C9CP06869D.

(71) Lu, T.; Chen, Q. Shermo: A General Code for Calculating Molecular Thermochemistry Properties. *Computational and Theoretical Chemistry* **2021**, *1200*, 113249. https://doi.org/10.1016/j.comptc.2021.113249.

(72) Grimme, S. Supramolecular Binding Thermodynamics by Dispersion-Corrected Density Functional Theory. *Chemistry – A European Journal* **2012**, *18* (32), 9955–9964. https://doi.org/10.1002/chem.201200497.

(73) Lu, T. *Concvar: A Computer Program for Simulating Concentration Variation of Complex Chemical Reactions*; preprint; Chemistry, 2022. https://doi.org/10.26434/chemrxiv-2022-r6rh8-v2.

TOC Graphic

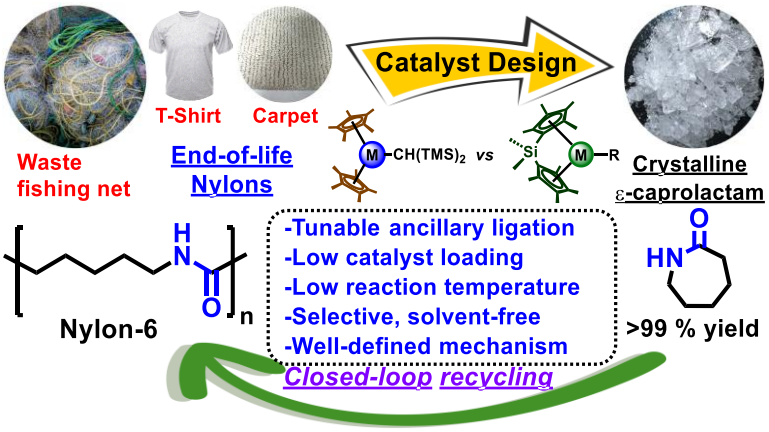
Waste fishing net
T-Shirt
Carpet
End-of-life Nylons
Catalyst Design
M–CH(TMS)2 vs Si M–R
Crystalline ε-caprolactam
Nylon-6
-Tunable ancillary ligation
-Low catalyst loading
-Low reaction temperature
-Selective, solvent-free
-Well-defined mechanism
>99 % yield
Closed-loop recycling